Rectilinearity Measurements for Polygons*

Joviša Žunić†, Paul L. Rosin

Computer Science Department, Cardiff University
Queen's Buildings, Newport Road, P.O. Box 916
Cardiff CF24 3XF, Wales, U.K.
e-mail: {J.Zunic, Paul.Rosin}@cs.cf.ac.uk

Abstract

The paper introduces a shape measure intended to describe the extent to which a closed polygon is rectilinear. Other than somewhat obvious measures of rectilinearity (e.g. the sum of the differences of each corner's angle from 90°) there has been little work in deriving a measure that is straightforward to compute, is invarient under scale and translation, and corresponds with the intuitive notion of rectilinear shapes.

There are applications in a number of different areas of computer vision and photogrammetry. Rectilinear structures often correspond to human-made structure, and are therefore justified as attentional cues for further processing. For instance, in aerial image processing and reconstruction, where building footprints are often rectilinear on the local ground plane, building structures, once recognized as rectilinear can be matched to corresponding shapes in other views for stereo reconstruction. Perceptual grouping algorithms may seek to complete shapes based on the assumption that the object is question is rectilinear. Using the proposed measure, such systems can verify this assumption.

Keywords: Shape, polygons, rectilinearity, measurement.

1 Introduction

Shape plays an important part in the processing of visual information, and is actively being investigated in a wide spectrum of areas, from art [24] through to science [7]. Within computer vision there have been many applications of shape to aid in the analysis of images, and standard shape descriptors include compactness, eccentricity [22], circularity [10], ellipticity [18], and rectangularity [19]. Many of these shapes are based on geometric patterns, which naturally closely correspond to many manufactured items (from ball bearings to skyscrapers), justifying their applicability. While their usefulness in the broader area of perception may be questioned, it has in fact been shown that regular shapes (e.g. rectangles versus general quadrilaterals) have particular significance in the human visual system [8].

This paper describes a shape measure that has received little attention: *rectilinearity*. While there exist a variety of approaches to computing the related measure of *rectangularity* [19], rectilinearity covers a wider space of shapes since the number of sides of the model shape is variable. This means that it is not convenient

*to appear in IEEE Trans. on Pattern Analysis and Machine Intelligence

†Joviša Žunić is also with the Mathematical Institute of the Serbian Academy of Sciences and Arts, Belgrade.

to fit the model[1] to the data and measure the discrepancies between the two, which is the approach that is often applied to compute compactness and rectangularity.

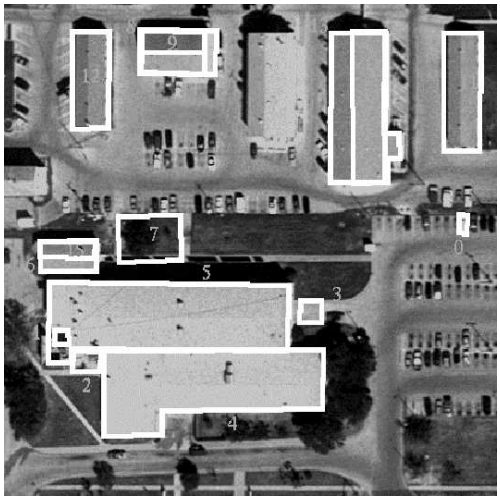

Figure 1: Automatic building detection by the Ascender II system [9].

One of our motivations in developing a rectilinearity shape measure is to provide a useful tool for the analysis of buildings in aerial photographs. Over the last 10–20 years there has been considerable research in this area with the goal of providing automatic photointerpretation which would be particularly useful for cartographers [12, 15, 17] – see for instance an example from the Ascender II system [4, 9] in Fig. 1. Such systems are typically based on perceptual grouping of edges and incorporate additional information such as shadows, colour, contextual information, miscellaneous knowledge-based rules, as well as shape (typically rectangular). Since many buildings appear rectilinear from an overhead view then such a shape measure could be used in a hypothesis and test paradigm to remove unlikely candidates which have inappropriate shapes. In addition to photointerpretation, detection of buildings can be used to provide control points for registration [11]. More generally, shape attributes have been used to select similar structures in image pairs to determine correspondences used to determine the image registration parameters. Dare *et al.* [5] suggested incorporating rectilinearity, although it was not implemented, while Ventura *et al.* [23] showed results in which eccentricity was employed.

As well as filtering out non-rectilinear shapes it is sometimes also useful to retain only non-rectilinear shapes. For example, in one study [21], in order to detect landslide induced changes between a time-lapsed pair of images, rectangular regions of change were eliminated since they arose from new buildings or fields with altered cultivation patterns. In general, distinguishing carpented artifacts from natural backgrounds is an obvious application.

Another set of applications relate to the modification of an input shape driven by the maximisation of the rectilinearity measure, and three instances are given here.

- **Shape from contour** – Brady & Yuille [1] determined 3D surface orientation from a 2D contour by deprojecting it so as to maximise the contour's compactness. In a similar manner, if it is known that the target shape is rectilinear, then the rectilinearity measure can replace compactness. It is interesting to note that whereas one of the assumptions of the statistical approach to shape from contour [26] is that

[1]Fitting a rectilinear shape *is* possible, as demonstrated by Brunn *et al.* [2], but is complex, and potentially unreliable and inaccurate. Other related work involves fitting x-monotonic rectilinear curves [6] and determining rectilinear paths whilst avoiding obstacles [3]. Our proposed approach avoids fitting, and is therefore simpler and faster.

the distribution of tangent angles along the curve is uniform, the rectilinear version works best under the opposite conditions.

- **Snakes** are used to refine an initial shape, optimising a function which most typically combines generic constrains such as smoothness as well as fidelity to the original data [14]. In certain applications it may be possible to include more specific constraints, such as a rectilinearity component, which are then likely to improve the object delineation/reconstruction.

- **Partitioning** – a simple scheme for partitioning shapes was developed using a weighted sum of the convexity of the subparts as the splitting criterion [20]. In most cases the results using the convexity measure seemed to match human perception. Again, in specific situations rectilinearity would be more appropriate, e.g. to separate adjoining rectilinear buildings whose boundaries have become merged somewhere in the image acquisition/precessing chain.

Let us conclude this introduction by noticing that a variety of rectilinearity measures for polygons which are based only on a measure of the angles of the considered polygon can be derived very easily. But such a defined rectilinearity measure would imply that all polygons with the same angles have the same estimated rectilinearity which is not acceptable. In view of example from Fig. 2 (a), the angles of $P(h)$ are $\frac{\pi}{2}, \frac{\pi}{2}, \frac{\pi}{2}, \frac{3\pi}{4}, \frac{3\pi}{4}$ for all $h \in (0,1)$, but it is natural to expect that polygons $P(h)$ for very small h (then $P(h)$ is "almost" a square) are more rectilinear than polygons $P(h)$ with h very close to 1 (then $P(h)$ is "almost" a triangle). Both rectilinearity measures introduced here agree that the rectilinearity of $P(h)$ decrease when h varies from 0 to 1 – the graphs of rectilinearity measures of $P(h)$ are displayed on Fig. 2, (b) and (c) (for more details see Section 4).

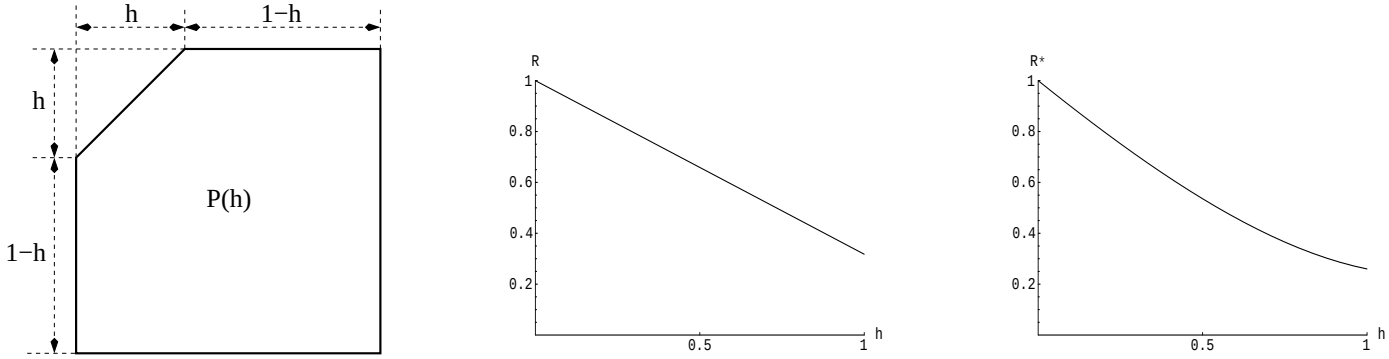

(a) (b) (c)

Figure 2: (a) Polygons $P(h)$ are expected to have the different measured rectilinearity when h varies from 0 (correspond to a square) to 1 (correspond to a triangle). (b) and (c) display the graphs of the rectilinearity of $P(h)$ measured by $\mathcal{R}_1$ and $\mathcal{R}_2$, respectively.

2 Definitions and Denotations

We start this section with a formal definition of rectilinear polygons (see Fig. 3 for an example).

Definition 2.1 *A polygon P is rectilinear if its interior angles belong to the set* $\left\{\frac{\pi}{2}, \frac{3\cdot\pi}{2}\right\}$.

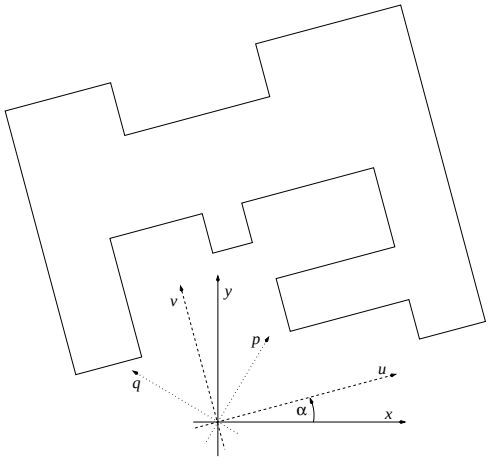

Figure 3: For the given rectilinear 20-gon P, its l_1 perimeter $\mathcal{P}er_1(P)$ has the minimum value if the coordinate axes are chosen to be parallel with u and v, while it reaches its maximum if the coordinate axes are parallel to p and q. The minimum and maximum values correspond to $\mathcal{P}er_1(P, 2\pi - \alpha)$ and $\mathcal{P}er_1(P, \frac{7\pi}{4} - \alpha)$, respectively, if x and y are taken to be the coordinate axes.

Also, we will use the following definitions and denotations (see Fig. 4 for some illustrations). The set of all polygons will be denoted by Π. For a given n-gon P having vertices denoted by $A_0, A_1, \ldots, A_{n-1}, A_n = A_0$, its edges will be denoted as $e_i = [A_{i-1}, A_i]$ for $i = 1, 2, \ldots, n$. The Euclidean length of the straight line segment $e = [(x_1, y_1), (x_2, y_2)]$ is $l_2(e) = \sqrt{(x_1 - x_2)^2 + (y_1 - y_2)^2}$, while the length of e according to the l_1 metric is $l_1(e) = |x_1 - x_2| + |y_1 - y_2|$.

$\mathcal{P}er_2(P)$ will denote the Euclidean perimeter of P, while $\mathcal{P}er_1(P)$ will denote the perimeter of P in the sense of l_1 metrics. So, $\mathcal{P}er_2(P) = \sum_{e_i \text{ is an edge of } P} l_2(e_i)$ and $\mathcal{P}er_1(P) = \sum_{e_i \text{ is an edge of } P} l_1(e_i)$. Since isometric polygons do not necessarily have the same perimeter under the l_1 metric, we shall use $\mathcal{P}er_1(P, \alpha)$ for the l_1 perimeter of the polygon which is obtained by the rotating P by the angle α with the origin as the center of rotation. If the same rotation is applied to the edge e, the l_1 perimeter of the obtained edge will be denoted as $l_1(e, \alpha)$.

If the oriented angle between the positively oriented x-axis and the vector $\overrightarrow{A_{i-1}A_i}$ is denoted by ϕ_i ($i = 1, 2, \ldots n$), then obviously $l_1(e_i, \alpha) = l_2(e_i) \cdot (|\cos(\phi_i + \alpha)| + |\sin(\phi_i + \alpha)|)$. Thus, by using $1 \leq |\cos\beta| + |\sin\beta| \leq \sqrt{2}$ (for any β), we have the next relations between $\mathcal{P}er_1(P)$ and $\mathcal{P}er_2(P)$.

$$\mathcal{P}er_2(P) = \sum_{i=1}^{n} l_2(e_i) \leq \mathcal{P}er_1(P, \alpha) = \sum_{i=1}^{n} l_2(e_i) \cdot (|\cos(\phi_i + \alpha)| + |\sin(\phi_i + \alpha)|) \leq \sqrt{2} \cdot \mathcal{P}er_2(P, \alpha) \quad (1)$$

Note 2.1 *Let us notice that $\mathcal{P}er_2(P) = \mathcal{P}er_1(P, \alpha)$ if and only if $|\cos(\phi_i + \alpha)| + |\sin(\phi_i + \alpha)| = 1$ holds for all edges e_i, $1 \leq i \leq n$. Analogously, $\mathcal{P}er_1(P) = \sqrt{2} \cdot \mathcal{P}er_1(P, \alpha)$ if and only if $|\cos(\phi_i + \alpha)| + |\sin(\phi_i + \alpha)| = \sqrt{2}$ holds for all edges e_i, $1 \leq i \leq n$.*

We will exploit a characterization of rectilinear polygons given by the next theorem.

Theorem 2.1 *A polygon P is rectilinear if and only if there exists α such that $\mathcal{P}er_1(P, \alpha) = \mathcal{P}er_2(P)$.*

Proof. If P is rectilinear then a rotation of P such that the edges of P become parallel to the coordinate axes preserves the equality $\mathcal{P}er_2(P) = \mathcal{P}er_1(P, \alpha)$, where α is the rotation angle.

On the other hand, $\mathcal{P}er_2(P) = \mathcal{P}er_1(P,\alpha)$ implies $|\cos(\phi_i+\alpha)| + |\sin(\phi_i+\alpha)| = 1$, or equivalently, either $\cos(\phi_i+\alpha) = 0$ or $\sin(\phi_i+\alpha) = 0$ for all edges e_i $(1 \le i \le n)$ of the given n-gon P. Consequently, we have that all edges of P are either parallel or orthogonal to the same line, i.e., P is rectilinear. ▯

3 The Basic Idea and Necessary Mathematics

Theorem 2.1 gives a useful characterisation of rectilinear polygons and gives the basic idea for the polygon rectilinearity measurement proposed in this paper. In the first stage, Theorem 2.1 together with $\mathcal{P}er_2(P) \le \mathcal{P}er_1(P)$ (see (1)) suggests that the ratio $\frac{\mathcal{P}er_2(P)}{\mathcal{P}er_1(P)}$ can be used as a rectilinearity measure for the polygon P. Precisely, $\frac{\mathcal{P}er_2(P)}{\mathcal{P}er_1(P)}$ has the following "good" properties:

a1) it is always a strictly positive number;

a2) it is defined for any polygon P;

a3) it can be calculated easily;

a4) for any non rectilinear polygon it is strictly less than 1 and for any given rectilinear polygon it is exactly 1 if the coordinate axes are suitable chosen.

But, on the other side $\frac{\mathcal{P}er_2(P)}{\mathcal{P}er_1(P)}$ has the following "bad" properties:

b1) it is not invariant under rotational transformations;

b2) the infimum for the set of values of $\mathcal{Q}_1(P,\alpha) = \frac{\mathcal{P}er_2(P)}{\mathcal{P}er_1(P,\alpha)}$ is not zero. For an example, it can be easily seen (from (1)) that there exists no polygon P such that $\frac{\mathcal{P}er_2(P)}{\mathcal{P}er_1(P)} \in \left(0, \frac{\sqrt{2}}{2}\right)$.

In this section we develop necessary mathematical tools in order to define a function which satisfies a1)–a5) but not b1) and b2).

The problems described by b1) can be avoided by considering $\max\limits_{\alpha\in[0,2\pi]} \frac{\mathcal{P}er_2(P)}{\mathcal{P}er_1(P,\alpha)}$ instead of $\frac{\mathcal{P}er_2(P)}{\mathcal{P}er_1(P)}$, but it opens the question of how to compute those maximum values. It turns out that can be designed a simple procedures for such calculations. It will described later – see Section 5.

Further, the inequalities from (1) give $\frac{\sqrt{2}}{2} \le \max\limits_{\alpha\in[0,2\pi]} \frac{\mathcal{P}er_2(P)}{\mathcal{P}er_1(P,\alpha)} \le 1$ for any polygon P. But, while the inequality $\frac{\mathcal{P}er_2(P)}{\mathcal{P}er_1(P)} \le 1$ is sharp, and moreover, the equality $\max\limits_{\alpha\in[0,2\pi]} \frac{\mathcal{P}er_2(P)}{\mathcal{P}er_1(P,\alpha)} = 1$ is satisfied if and only if P is a rectilinear polygon (due to Theorem 2.1), it can be easily seen that there exists no polygon P such that $\max\limits_{\alpha\in[0,2\pi]} \frac{\mathcal{P}er_2(P)}{\mathcal{P}er_1(P,\alpha)} = \frac{\sqrt{2}}{2}$. Namely, if an n-gon P satisfies the last equality, then for some α_0 we have $\frac{\mathcal{P}er_2(P)}{\mathcal{P}er_1(P,\alpha_0)} = \frac{\sqrt{2}}{2}$ which (by (1)) would imply $\sqrt{2}\cdot l_2(e_i) = l_1(e_i,\alpha_0)$ or, equivalently, $\phi_i + \alpha_0 \in \{\pi/4, 3\pi/4, 5\pi/4, 7\pi/4, 9\pi/4, 11\pi/4, \}$ for any edge e_i where $1 \le i \le n$. Thus, P must be rectilinear, and due to Theorem 2.1, the considered maximum must be equal to 1, which is a contradiction.

So, for our purpose it is necessary to determine the maximal possible μ such that $\max\limits_{\alpha\in[0,2\pi]} \dfrac{\mathcal{P}er_2(P)}{\mathcal{P}er_1(P,\alpha)}$ belongs to the interval $[\mu, 1]$ for any polygon P. The next lemma shows that $\mu = \frac{\pi}{4}$, and moreover, there is no polygon P such that $\max\limits_{\alpha\in[0,2\pi]} \frac{\mathcal{P}er_2(P)}{\mathcal{P}er_1(P,\alpha)} = \frac{\pi}{4}$.

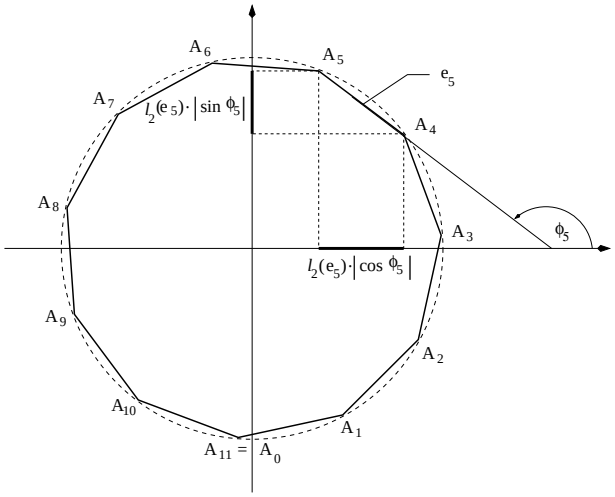

Figure 4: A regular 11-gon inscribed into the unit circle with the center placed at the origin.

Lemma 3.1 **a)** *The inequality* $\max\limits_{\alpha\in[0,2\pi]} \frac{\mathcal{P}er_2(P)}{\mathcal{P}er_1(P,\alpha)} > \frac{\pi}{4}$ *holds for any polygon* P.

b) *For any* $\varepsilon > 0$ *there is a polygon* P *such that* $\max\limits_{\alpha\in[0,2\pi]} \frac{\mathcal{P}er_2(P)}{\mathcal{P}er_1(P,\alpha)} < \frac{\pi}{4} + \varepsilon$, *or equivalently*

$$\inf_{P\in\Pi} \left\{ \max_{\alpha\in[0,2\pi]} \frac{\mathcal{P}er_2(P)}{\mathcal{P}er_1(P,\alpha)} \right\} = \frac{\pi}{4}.$$

Proof. We prove the statement **a)** by a contradiction. Let us assume the contrary, i.e., there exists an n-gon P such that $\frac{\mathcal{P}er_2(P)}{\mathcal{P}er_1(P,\alpha)} \leq \frac{\pi}{4}$ or equivalently, $\frac{\mathcal{P}er_1(P,\alpha)}{\mathcal{P}er_2(P)} \geq \frac{4}{\pi}$ for any $\alpha \in [0, 2\pi]$. Since $\frac{\mathcal{P}er_1(P,\alpha)}{\mathcal{P}er_2(P)}$ is a continuous non constant function (for more details see Section 5) depending on α (if P is fixed), and since it is assumed to be greater or equal to $\frac{4}{\pi}$ then $\int_0^{2\pi} \frac{\mathcal{P}er_1(P,\alpha)}{\mathcal{P}er_2(P)} \cdot d\alpha > \int_0^{2\pi} \frac{4}{\pi} \cdot d\alpha = 8$. Using the last inequality we derive:

$$8 < \int_0^{2\pi} \frac{\mathcal{P}er_1(P,\alpha)}{\mathcal{P}er_2(P)} \cdot d\alpha = \frac{1}{\mathcal{P}er_2(P)} \cdot \int_0^{2\pi} \left(\sum_{i=1}^{n} l_1(e_i,\alpha) \right) \cdot d\alpha = \frac{1}{\mathcal{P}er_2(P)} \cdot \sum_{i=1}^{n} \left(\int_0^{2\pi} l_1(e_i,\alpha) \cdot d\alpha \right)$$

$$= \frac{1}{\mathcal{P}er_2(P)} \cdot \sum_{i=1}^{n} \left(\int_0^{2\pi} l_2(e_i) \cdot (|\sin(\phi_i+\alpha)| + |\cos(\phi_i+\alpha)|) \cdot d\alpha \right) = \frac{1}{\mathcal{P}er_2(P)} \cdot \left(\sum_{i=1}^{n} 8 \cdot l_2(e_i) \right) = 8.$$

The obtained contradiction $8 < 8$ proves **a)**.

To prove the statement **b)** it is enough to find a sequence of polygons $P_3, P_4, P_5, \ldots$ such that $\lim\limits_{n\to\infty} \left(\max\limits_{\alpha\in[0,2\pi]} \frac{\mathcal{P}er_2(P}{\mathcal{P}er_1(P_n} \right.$ $\frac{\pi}{4}$. We will prove that the sequence of regular n-gons P_n inscribed into the unit circle satisfies the previous equality. Namely, it can be easily seen that the sequence of the Euclidean perimeters of P_n tends to the perimeter of the unit circle, i.e., $\lim_{n\to\infty} \mathcal{P}er_2(P_n) = 2 \cdot \pi$ but also $\lim_{n\to\infty} \mathcal{P}er_1(P_n,\alpha) = 8$ holds independently on the choice of α. Precisely, if it is considered that (for any $\alpha \in [0, 2\pi]$) the l_1 perimeter $\mathcal{P}er_1(P_n,\alpha)$ equals the sum of the projections of all edges of P_n onto x and y axes, than it follows that this sum tends to 8 as $n \to \infty$ (see Fig. 4 for an illustration). Since two last limits are independent on α we have $\lim_{n\to\infty} \frac{\mathcal{P}er_2(P_n)}{\mathcal{P}er_1(P_n,\alpha)} = \lim_{n\to\infty} \left(\max_{\alpha\in[0,2\pi]} \frac{\mathcal{P}er_2(P_n)}{\mathcal{P}er_1(P_n,\alpha)} \right) = \frac{\pi}{4}$, what proves **b)**. ∎

4 Rectilinearity Measures

Motivated by the proved properties of the function $\max\limits_{\alpha\in[0,2\pi]} \frac{\mathcal{P}er_2(P)}{\mathcal{P}er_1(P,\alpha)}$ we give the following definition for the new rectilinearity measurement of polygons.

Definition 4.1 *For an arbitrary polygon P we define its rectilinearity $\mathcal{R}_1(P)$ as*

$$\mathcal{R}_1(P) \;=\; \frac{4}{4-\pi}\cdot\left(\max_{\alpha\in[0,2\pi]}\frac{\mathcal{P}er_2(P)}{\mathcal{P}er_1(P,\alpha)}-\frac{\pi}{4}\right)\,.$$

The following theorem summarises the properties of the polygon rectilinearity measure proposed here.

Theorem 4.1 *For any polygon P, we have:*

i) $\mathcal{R}_1(P)$ *is well defined and* $\mathcal{R}_1(P)\in(0,1]$ *for any polygon P;*

ii) $\mathcal{R}_1(P)=1$ *if and only if* P *is rectilinear;*

iii) $\inf\limits_{P\in\Pi}(\mathcal{R}_1(P))=0$*;*

iv) $\mathcal{R}_1(P)$ *is invariant under similarity transformations.*

Proof. For a fixed P, $\frac{\mathcal{P}er_2(P)}{\mathcal{P}er_1(P,\alpha)}$ is a continuous function depending on α (for more details see the next section). Consequently, it must reach its minimum on the closed interval $[0,2\pi]$, i.e., $\mathcal{R}_1(P)$ is well defined. $\mathcal{R}_1(P)\in(0,1]$ follows from (1), Definition 4.1, and Lemma 3.1.
The item *ii)* is a direct consequence of Theorem 2.1.
The item *iii)* is the statement of Lemma 3.1.
To prove *iv)* let us notice that $\mathcal{R}_1(P)$ is invariant under all isometric transformations – which follows from the definition. Also, $\frac{\mathcal{P}er_2(P)}{\mathcal{P}er_1(P,\alpha)}$ and consequently $\mathcal{R}_1(P)$ are invariant under any transformation of the form $(x,y)\to(\lambda\cdot x,\lambda\cdot y)$ for any choice of $\lambda\neq 0$, P, and α. That completes the proof. ▥

Let us conclude this section mentioning that starting form $\frac{\sqrt{2}}{2}\le\frac{\mathcal{P}er_1(P)}{\sqrt{2}\cdot\mathcal{P}er_2(P)}\le 1$ (see (1)) another rectilinearity measure can be derived. We give the next theorem without proof.

Theorem 4.2 *Let us define the rectilinearity measure for polygons in the following way*

$$\mathcal{R}_2(P) \;=\; \frac{\pi}{\pi-2\cdot\sqrt{2}}\cdot\left(\max_{\alpha\in[0,2\pi]}\frac{\mathcal{P}er_1(P,\alpha)}{\sqrt{2}\cdot\mathcal{P}er_2(P)}-\frac{2\cdot\sqrt{2}}{\pi}\right). \tag{2}$$

Then i) $\mathcal{R}_2(P)$ *is well defined and* $\mathcal{R}_2(P)\in(0,1]$*, ii)* $\mathcal{R}_2(P)=1$ *if and only if* P *is rectilinear, iii)* $\inf\limits_{P\in\Pi}(\mathcal{R}_2(P))=0$*, and iv)* $\mathcal{R}_2(P)$ *is invariant under similarity transformations.*

Let us go back to the example of the polygon $P(h)$ from Fig. 2. Elementary mathematics shows that $\min\limits_{\alpha\in[0,2\pi]}\mathcal{P}er_1(P(h),\alpha)=4$ for any $h\in[0,1]$ and $\max\limits_{\alpha\in[0,2\pi]}\mathcal{P}er_1(P(h),\alpha)=2\cdot\sqrt{8-4\cdot h+h^2}$ for $h\in[0,1]$. Also, $\mathcal{P}er_2(P(h))=4-(2-\sqrt{2})\cdot h$ if $h\in[0,1]$. Based on this, $\mathcal{R}_1(P(h))=1-\frac{(2-\sqrt{2})\cdot h}{4-\pi}$, i.e., $\mathcal{R}_1(P(h))$ behaves as a linear function which reaches its maximum 1 for $h=0$ ($P(0)$ corresponds to a square) and reaches the minimum $\frac{2+\sqrt{2}-\pi}{4-\pi}\approx 0.3176$ for $h=1$ ($P(1)$ corresponds to a triangle). Also, $\mathcal{R}_2(P(h))=\frac{\pi}{\pi-2\cdot\sqrt{2}}\cdot\left(\frac{2\cdot\sqrt{8-4\cdot h+h^2}}{\sqrt{2}\cdot(4-(2-\sqrt{2})\cdot h)}-\frac{2\cdot\sqrt{2}}{\pi}\right)$ and decrease from $1=\mathcal{R}_2(P(0))$ to $\mathcal{R}_2(P(1))\approx 0.2598$.

As shown above, the rectilinearity measures $\mathcal{R}_1$ and $\mathcal{R}_2$ are different. Moreover, as the examples of their application to synthetic (see Fig. 5) and real (see Fig. 11) polygons demonstrate, they produce different rankings. Nevertheless, we are not able to give a preference for either one, since both have the same computational complexity and match against human performance (see Section 7) to roughly the same degree.

5 Computation of $\mathcal{R}_1(P)$

In this section we will show how to compute $\mathcal{R}_1(P)$ effectively if a polygon P is given. Since $\mathcal{P}er_2(P)$ can be easily calculated from the vertices of P it remains to describe the computation of the minimum value of $\mathcal{P}er_1(P,\alpha)$ (necessary for the computation of $\mathcal{R}_1(P)$).

Let an edge e_i $(1 \leq i \leq n)$ of a given n-gon P be given. Trivially,
$l_1(e_i,\alpha) = l_2(e_i)\cdot(|\cos(\phi_i+\alpha)| + |\sin(\phi_i+\alpha)|) = a(\alpha)\cdot l_2(e_i)\cdot\cos(\phi_i+\alpha) + b(\alpha)\cdot l_2(e_i)\cdot\sin(\phi_i+\alpha)$ where $a(\alpha)$ and $b(\alpha)$ take $+1$ or -1 depending on α. Consequently, there is an integer k and a sequence $0 \leq \alpha_1 < \alpha_2 < \ldots < \alpha_k \leq 2\pi$ such that

$$\mathcal{P}er_1(P,\alpha) = \sum_{i=1}^{n} a_{j,i}\cdot l_2(e_i)\cdot\cos(\phi_i+\alpha) + b_{j,i}\cdot l_2(e_i)\cdot\sin(\phi_i+\alpha) \qquad \text{if } \alpha\in[\alpha_j,\alpha_{j+1}] \tag{3}$$

where $\alpha_{k+1} = \alpha_1 + 2\pi$ and $\{a_{j,i}, b_{j,i} \mid 1\leq j\leq k,\ 1\leq i\leq n\} \subset \{+1,-1\}$.

Note 5.1 *For any angle $\alpha_p \in \{\alpha_1,\alpha_2,\ldots,\alpha_k\} \subset [0,\ 2\pi]$ there is an edge e_q, $1\leq q\leq n$ such that the rotation of e_q for the angle α_p belong to one of coordinate axes – so, $k \leq 4\cdot n$. Since some of such angles can coincide, depending of the given n-gon the inequality $k \leq 4\cdot n$ can be strict.*

What is important for us is the next consequence of (3): $0 < \mathcal{P}er_1(P,\alpha) = -\mathcal{P}er_1''(P,\alpha)$ if $\alpha \notin \{\alpha_1,\alpha_2,\ldots,\alpha_k\}$, which implies that $\mathcal{P}er_1(P,\alpha)$ does not have any local minimum inside the open intervals: $(\alpha_1,\alpha_2),\ (\alpha_2,\alpha_3),\ \ldots,\ (\alpha_{k-1},\alpha_k),\ (\alpha_k, 2\pi+\alpha_1)$. In other words, we have $\min\limits_{\alpha\in[0,2\pi]} \mathcal{P}er_1(P,\alpha) = \min\{\mathcal{P}er_1(P,\alpha_1),\ \mathcal{P}er_1(P,\alpha_2),\ \ldots,\ \mathcal{P}er_1(P,\alpha_{k-1}),\ \mathcal{P}er_1(P,\alpha_k)\}$, which proves the following theorem.

Theorem 5.1 *For a given polygon P its measured rectilinearity $\mathcal{R}_1(P)$ can be computed as*

$$\mathcal{R}_1(P) = \frac{4}{4-\pi}\cdot\left(\frac{\mathcal{P}er_2(P)}{\min\{\mathcal{P}er_1(P,\alpha_1),\ \mathcal{P}er_1(P,\alpha_2),\ \ldots,\ \mathcal{P}er_1(P,\alpha_{k-1}),\ \mathcal{P}er_1(P,\alpha_k)\}} - \frac{\pi}{4}\right).$$

The previous theorem shows that the rectilinearity of a given n-gon (even defined by using the maximum value of a nonlinear function on an interval domain) can be computed by comparing easily computable values in at most $4\cdot n$ points. A straightforward application of Theorem 5.1 gives $O(n^2)$ as an upper bound for $\mathcal{R}_1(P)$ computation. In practise, for $n = 2500$ $\mathcal{R}_1(P)$ is calculated within 5 milliseconds on a Sun Ultra 10 workstation.

6 Some Examples

To test the effectiveness of the rectilinearity measures they are first applied to a (perfect) rectilinear polygon located as the top left hand shape in Fig. 5 which is then degraded in various ways. The first row demonstrates the effect of increasing levels of local noise applied to the polygon's vertices. In the second row the polygon is edited, eliminating vertices, which effectively rounds corners and increases its convexity. A shearing transformation is applied in the third row. Finally, the polygon is warped, and the axis aligned edges are increasingly rounded. All examples show that the rectilinearity measure is well behaved; increasing distortion consistently decreases the computed value. Note also that the orientations that maximised $\mathcal{Q}_1(P,\alpha) = \frac{\mathcal{P}er_2(P)}{\mathcal{P}er_1(P,\alpha)}$ match our expectations except at high noise levels when the rectilinearity measure has dropped close to zero. Also of note is the difference in orientation of skewed rectilinear shapes as determined by $\mathcal{R}_1$ and $\mathcal{R}_2$. Whilst $\mathcal{R}_1$ aligns one of the shape's edge orientations with the axis it can be shown that $\mathcal{R}_2$ consistently places the

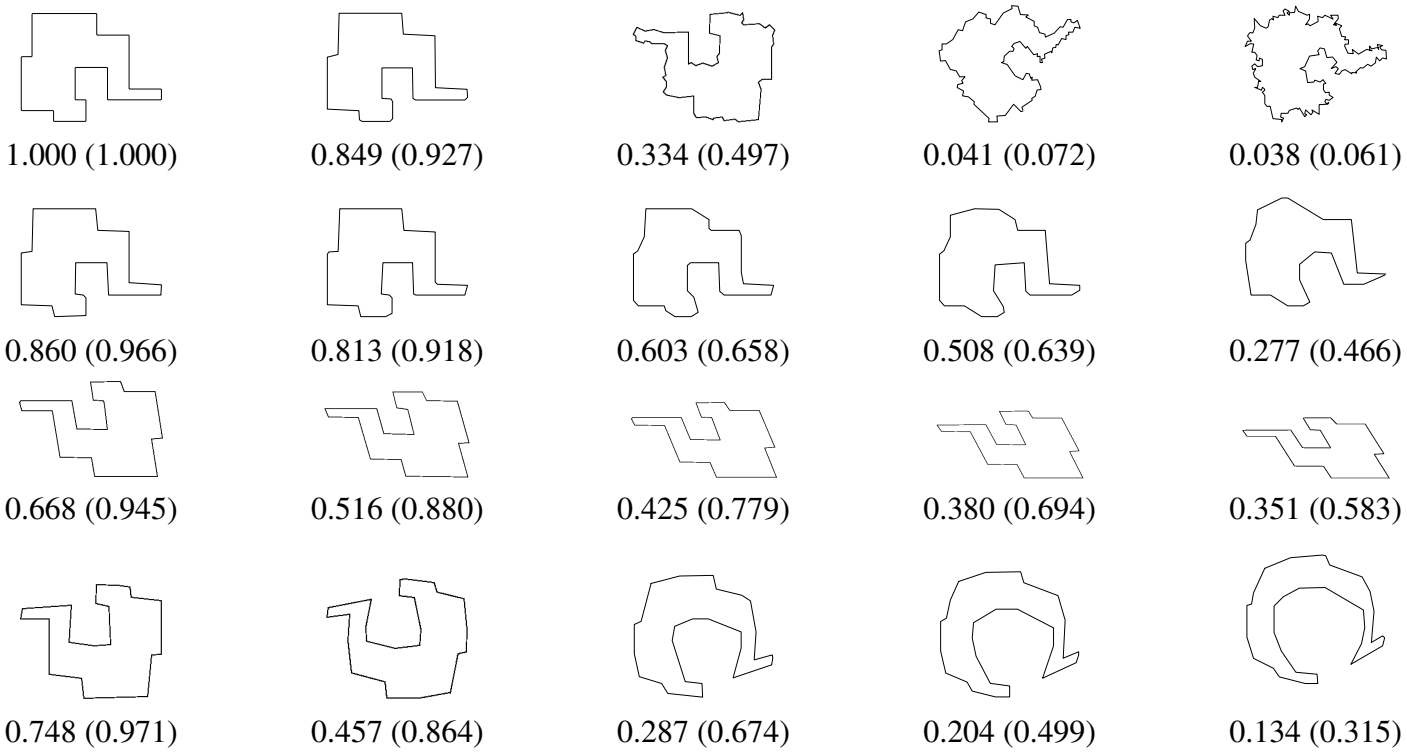

Figure 5: Examples of polygons rotated to the orientations that maximised $\mathcal{Q}_1(P, \alpha)$. Underneath are the rectilinearity values measured using $\mathcal{R}_1$, with the $\mathcal{R}_2$ values in brackets.

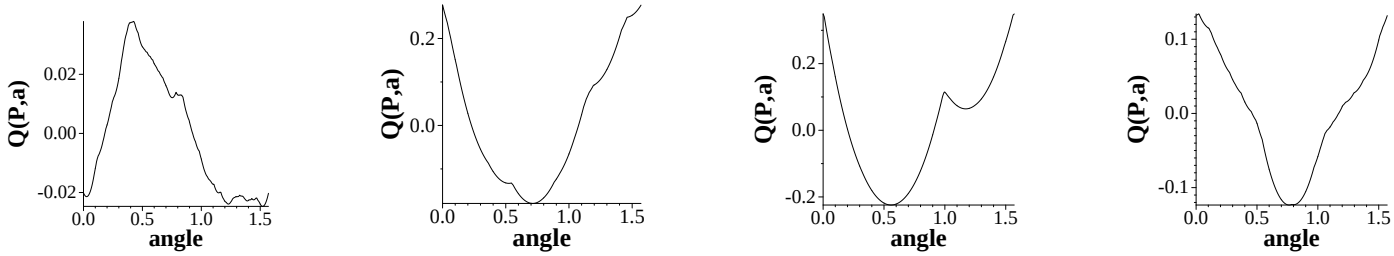

Figure 6: Plots of normalised $\mathcal{Q}_1(P, \alpha)$ for each of the rightmost examples in Fig. 5.

shape's axis in between the two edge orientations. For each of the maximally degraded polygons (i.e. the rightmost examples in each row) Fig. 6 plots $\mathcal{Q}_1(P, \alpha)$. It can be seen that it is well behaved and, despite the effects of noise and other distortions which introduce local maxima, the main peak remains distinct.

Another example is shown, applied to real data from a Digital Elevation Model (DEM), i.e., a depth map (see Fig. 7 (a)). Simple noise filtering and segmentation techniques were applied to produce a set of polygons. Fig. 7 (b) plots the regions filled with intensities proportional to their rectilinearity ($\mathcal{R}_1$); thus rectilinear shapes should appear bright. In some cases the computed rectilinearity does not correspond well with human perception. The problem arises from errors in the boundary due to the various steps in data processing, resulting in the distribution of edge orientation being fairly uniform, therefore producing a low rectilinearity value.

As a possible means of reconciling this inconsistency between our perceptual and measured evaluation of rectilinearity we note that relatively small adjustments to the polygon could greatly increase the values of $\mathcal{Q}_1(P)$. Thus we apply such a process, moving vertices such that they maximise $\mathcal{Q}_1(P)$ while minimising the

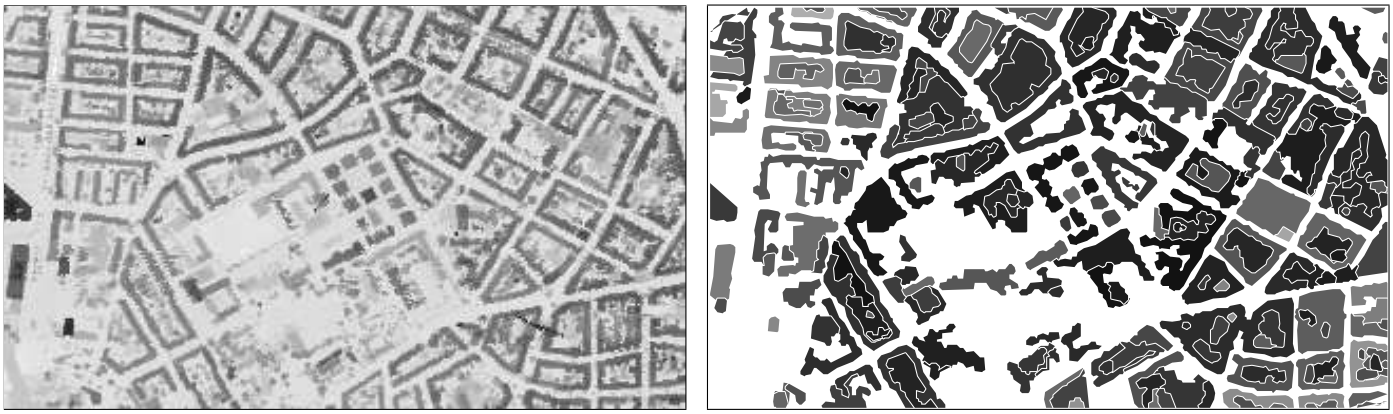

(a) (b)

Figure 7: (a) A DEM of Hanover; (b) segmented regions with intensities proportional to $\mathcal{R}_1$ rectilinearity.

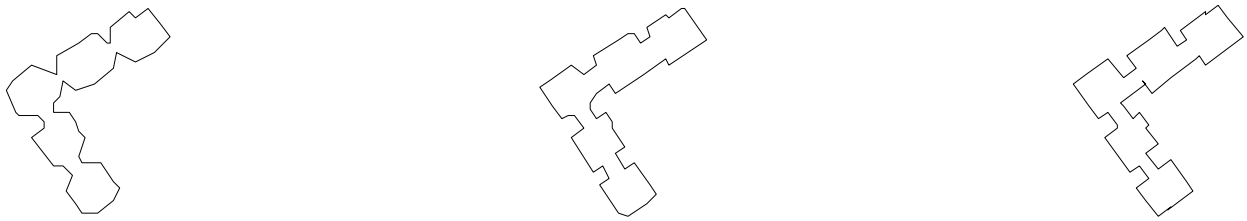

$\omega = 0.3$; $\mathcal{R}_1 = 0.236$ $\omega = 0.6$; $\mathcal{R}_1 = 0.748$ $\omega = 1.0$; $\mathcal{R}_1 = 0.891$

Figure 8: Evolved snakes with different weighting factors. Increasing ω produces greater rectilinearity.

shift in vertex location. This is a version of the popular snake methodology, but with a more specifically shape based internal force than the usual smoothness term. A similar scheme of "shape correction" has already been applied by Brunn *et al.* [2] who applied an iterative MDL vertex shifting and removal scheme, and by Mayer [16] who used constrained snakes. Our approach is rather simpler: it uses the greedy algorithm [25] and at each trial vertex shift computes the rectilinearity $\mathcal{R}_1$ and the mean distance D between the original and adjusted curve which are combined as the functional to be maximised: $F(\omega) = \omega\mathcal{R}_1 - (1-\omega)D$, where ω is a weighting term specifying the relative importance between the two terms. The effects of enforcing increasing degrees of rectilinearity on a building from Fig. 7 are shown in Fig. 8. Applying the snake-based rectilinearity process to the full set of regions in Fig. 7 is given for two values of ω in Fig. 9.

A final example is taken from the trademark retrieval study by Jain and Vailaya [13]. From a database of 1100 binary trademark images a human drawn query (boxed trademark in Fig. 10 (a)) was input. The top ranked images according to five human subjects [13] are shown in Fig. 10 (a). Beyond the obvious best matched image the remaining images show the difficulty caused by the subjective nature of the task. Jain and Vailaya find an initial match using a distance made up from a weighted combination of the dissimilarities computed from the edge histogram and the first seven moment invariants (Fig. 10 (b)). They continue to refine the match using a deformable template, region filling, etc. We compare their initial results against the following set of simple shape descriptors: circularity, ellipticity, the first four moment invariants, and the circularity, ellipticity, triangularity, and aspect ratio of the convex hull. Matching was performed using a normalised Euclidean distance classifier in which the convex hull measures were downweighted a quarter relative to the other measures. Fig. 10 (c) shows that the correct match is found in second place. The addition

(a) $\omega = 0.3$ (b) $\omega = 0.6$

Figure 9: Applying rectilinear snakes to "correct" the regions from Fig. 7 in order to improve rectilinearity (measured by $\mathcal{R}_1$). Regions intensities are proportional to rectilinearity.

of rectilinearity improves performance (Fig. 10 (d)); not only does the correct match move from second to first place, but amongst the remaining matches there is now another from the human ground truth set. Moreover, the sixth ranked shape is also qualitatively similar to the bull.

(a) Hand drawn trademark query (boxed) and the top nine images retrieved by human subjects

(b) Top ten images retrieved by Jain and Vailaya's pruning stage

(c) Top ten images using simple shape descriptors

(d) Top ten images using simple shape descriptors plus rectilinearity

Figure 10: Top ten retrieved trademarks

7 Comparison against Human Perception

Having defined new computational schemes for measuring rectilinearity it is of interest to check how they compare against human perception. 22 human subjects were asked to rank order the 37 shapes in Fig. 11 according to rectilinearity.[2] The average rank for each shape over the human subjects was calculated, and the

[2]The subjects were naive adults. The concept of rectilinearity was explained to them in two ways: a perfect rectilinear shape could be composed of horizontal and vertical lines if oriented appropriately; alternatively, the internal angles should be $\pm 90°$. No

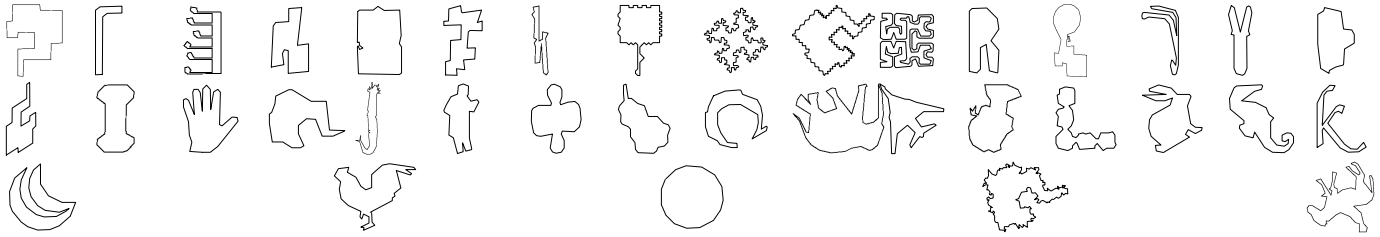

(a) $\mathcal{R}_1$

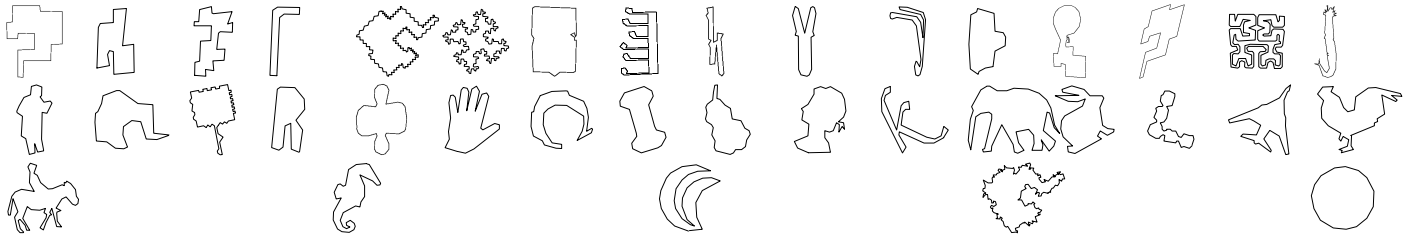

(b) $\mathcal{R}_2$

Figure 11: Shapes ranked by rectilinearity measures.

shapes sorted accordingly are displayed in Fig. 12. The average rank of each shape is shown in Fig. 13 (sorted into ascending order) and the error bars show that there was substantial variability in the human rankings. It is interesting to note that the first five shapes have lower errors and form a group that was considered to be more readily discernible as rectilinear. They also closely match the computer generated rankings. The last three or four shapes can also be seen to stand out as being more definitely non-rectilinear. This matches up with the comments from many of the subjects that they had difficulty in performing accurate ordering of the large middle group of shapes.

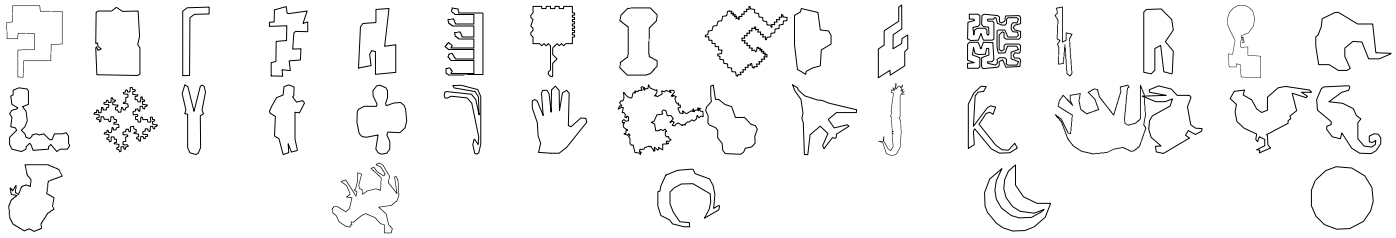

Figure 12: Shapes sorted by mean human subject ranking

A more quantitative analysis was carried out by calculating the Spearman rank-order correlation coefficient. Comparing the scores of the human subjects against the mean human ranking produced a correlation coefficient of 0.799 with standard deviation 0.086. Comparing the measures described in this paper against the mean human ranking produced: 0.886 ($\mathcal{R}_1$), 0.815 ($\mathcal{R}_2$), demonstrating that the algorithms are consistent with human perception. Despite the variability in the rankings all the results (human and computer) exhibit high correlation against the mean human ranking (at the 0.01 significance level).

time limit was given, and the task typically took about five minutes. The shapes were presented as circular cut outs, randomly laid out so that there was no initial preferred orientation or ordering.

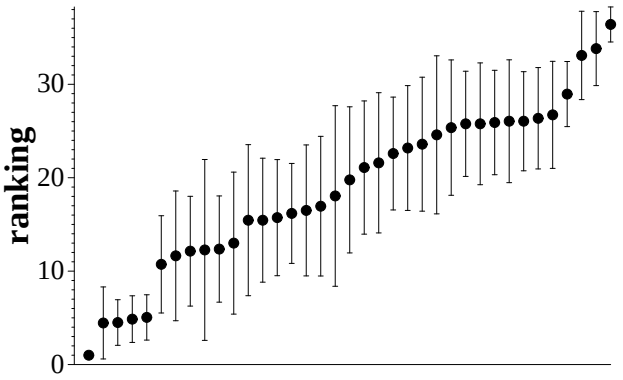

Figure 13: Mean ranking of the 37 shapes in figures 11 according to 22 human subjects. Error bars are marked at one standard deviation.

8 Concluding Remarks

This paper has looked at the problem of efficiently measuring the rectilinearity of polygons. Based on a simple characterisation of rectilinear polygons two rectilinearity measures for polygons have been defined. Although $\mathcal{R}_1(P)$ and $\mathcal{R}_2(P)$ are derived from the same source and give similar results, they are indeed different. Thus in Fig. 11, while there are substantial similarities and the mean difference in rank is only about two or three, many individual differences are evident. Tests showed that both correspond well with human judgement of rectilinearity.

The results presented have concentrated on the application of the measures to individual polygons. However, when applying $\mathcal{R}_1(P)$ and $\mathcal{R}_2(P)$ to sets of polygons extracted from an image the result will be dependent on how the image is clustered into polygons in the first place. In such situations the rectilinearity measure can be used to drive an appropriate grouping (i.e. selection) from the image polygon set.

Acknowledgments

The authors would like to Aditya Vailaya for providing the trademark database and Uwe Weidner for providing the DEM.

References

[1] M. Brady and A.L. Yuille. An extremum principle for shape from contour. *IEEE Trans. on Pattern Analysis and Machine Intelligence*, 6(3):288–301, 1984.

[2] A. Brunn, U. Weidner, and W. Förstner. Model-based 2d-shape recovery. In G. Sagerer et al, editor, *Mustererkennung*, pages 260–268. Springer-Verlag, 1995.

[3] D. Chen and J. Xu. An efficient direct approach for computing shortest rectilinear paths among obstacles in a two-layer interconnection model. *Computational Geometry: Theory and Applications*, 18:155–166, 2001.

[4] R.T. Collins, C.O. Jaynes, Y.Q. Cheng, X.G. Wang, F.R. Stolle, E.M. Riseman, and A.R. Hanson. The Ascender system: Automated site modeling from multiple aerial images. *Computer Vision and Image Understanding*, 72(2):143–162, 1998.

[5] P.M. Dare, R. Ruskoni, and I.J. Dowman. Algorithm development for the automatic registration of satellite images. In *Proc. Image Registration Workshop, NASA Goddard Space Flight Centre*, pages 83–88, 1997.

[6] J.M. Díaz-Baqez and J.A. Mesa. Fitting rectilinear polygonal curves to a set of points in the plane. *European J. Oper. Res.*, 130(1):214–222, 2001.

[7] S. Hyde *et al. The Language of Shape*. Elsevier, 1997.

[8] J Feldman. Bias toward regular form in mental shape spaces. *Journal of Experimental Psychology: Human Perception*, 26(1):1–14, 2000.

[9] A.R. Hanson, M. Marengoni, H. Schultz, F. Stolle, and E.M. Riseman. Ascender II: A framework for reconstruction of scenes from aerial images. In *Intl. Workshop on Aerial and Spaceborne Imagery*, pages 25–34, 2001.

[10] R.M. Haralick. A measure for circularity of digital figures. *IEEE Trans. on Systems, Man and Cybernetics*, 4:394–396, 1974.

[11] Y.C. Hsieh, D.M. McKeown, Jr., and F.P. Perlant. Performance evaluation of scene registration and stereo matching for cartographic feature extraction. *IEEE Trans. on Pattern Analysis and Machine Intelligence*, 14(2):214–238, 1992.

[12] R.B. Irvin and D.M. McKeown. Methods for exploiting the relationship between buildings and their shadows in aerial imagery. *IEEE Trans. on Systems, Man and Cybernetics*, 19(6):1564–1575, 1989.

[13] A.K. Jain and A. Vailaya. Shape-based retrieval: A case-study with trademark image databases. *Pattern Recognition*, 31(9):1369–1390, 1998.

[14] M. Kass, A. Witkin, and D. Terzopoulos. Snakes: active contour models. In *Int. Conf. Computer Vision*, pages 259–268, 1987.

[15] Y.T. Liow and T. Pavlidis. Use of shadows for extracting buildings in aerial images. *Computer Vision, Graphics and Image Processing*, 49(2):242–277, 1990.

[16] S. Mayer. Constrained optimization of building contours from high-resolution ortho-images. In *Proc. Int. Conf. Image Processing*, 2001.

[17] S. Noronha and R. Nevatia. Detection and modeling of buildings from multiple aerial images. *IEEE Trans. on Pattern Analysis and Machine Intelligence*, 23(5):501–518, 2001.

[18] D. Proffitt. The measurement of circularity and ellipticity on a digital grid. *Pattern Recognition*, 15(5):383–387, 1982.

[19] P.L. Rosin. Measuring rectangularity. *Machine Vision and Applications*, 11:191–196, 1999.

[20] P.L. Rosin. Shape partitioning by convexity. *IEEE Trans. on Systems, Man and Cybernetics*, part A, 30(2):202–210, 2000.

[21] P.L. Rosin and J. Hervás. Remote sensing image thresholding for determining landslide activity. *Int. J. Remote Sensing*, in press.

[22] M. Sonka, V. Hlavac, and R. Boyle. *Image Processing, Analysis, and Machine Vision*. Chapman and Hall, 1993.

[23] A.D. Ventura, A. Rampini, and R. Schettini. Image registration by recognition of corresponding structures. *IEEE Trans. on Geoscience and Remote Sensing*, 28(3):305–314, 1990.

[24] J. Willats. *Art and Representation: New Principles in the Analysis of Pictures*. Princeton University Press, 1997.

[25] D. Williams and M. Shah. Greedy algorithm for activecontour and curvature estimation. *Computer Vision, Graphics and Image Processing*, pages 14–26, 1992.

[26] A. Witkin. Shape from contour. Technical Report 589, MIT, 1980.